True Myocardial Motion Tracking

Stefan E. Fischer, Graeme C. McKinnon, Markus B. Scheidegger, Wim Prins, Dieter Meier, Peter Boesiger

Myocardial tagging is a powerful tool for the assessment of in-plane cardiac motion. However, for previous myocardial tagging techniques, the imaged slice is fixed with respect to the magnet coordinate system. Thus, images acquired at different heart phases do not always represent the same slice of the myocardium. A new myocardial tagging technique is presented, which takes the through-plane motion into consideration. It involves tagging of the desired myocardial slice and applying a subtraction imaging technique to image just that part of the myocardium. The examination time can be reduced considerably by the acquisition of two one-dimensionally tagged images. To increase the signal-to-noise ratio especially at later heart phases, variable imaging RF excitation flip angles are applied. To reduce motion artifacts a repetitive breathhold scheme was applied. *In vivo* results demonstrate that the tags can be accurately tracked within the entire heart period with a temporal resolution of 35 ms, even at a top basal level of the heart and right ventricle.

Key words: cardiac MRI; myocardial tagging; spatial modulation of the magnetization (SPAMM); cardiac motion.

INTRODUCTION

Myocardial tagging (1, 2) is a powerful tool for the assessment of in-plane cardiac motion (3, 4). During systole a shortening and a thickening of the myocardium are observed on short-axis images, superimposed by a clockwise and a counterclockwise rotation at the basal and apical levels of the heart, respectively (5). In addition to this wringing motion, a contraction parallel to the long axis occurs, such that the base moves toward the apex. This displacement can be about 2 to 2.2 cm for the left (6) and even more for the right ventricle (7) and depends on the myocardial segment and on its position with respect to the long axis. For a highly accurate description of the motion, as is required for any estimation of strain (8), the motion in the third dimension (i.e., the through-plane motion) has to be taken into consideration. One approach for the assessment of the three-dimensional motion consists of the acquisition and the evaluation of two orthogonal stacks of tagged images. After identification of the tagging pattern on each image of the two stacks, an interpolation procedure is applied to generate the three-dimensional myocardial motion map (9). Using this approach the deformation of the tagging grid is extracted for a selected plane and for a selected imaging time point. To obtain the displacement of the tagged tissue, the trajectory has to be followed in the reverse time direction, and one has to search for the same labeled point within a stack of images. Thus, tracking a specific point of the myocardium through the cardiac cycle requires much image processing and interpolation, and cannot be performed on a multiple phase image series from a single slice.

For cardiac imaging a method has been proposed (6) that allows one to follow an initially selected thin slice, provided it remains within a thicker imaged volume. The slice isolation is obtained by the application of slice-selective RF presaturation pulses parallel to the imaged slice. This presaturation procedure can be combined with a preceding tagging sequence. However, it can only be optimized for one particular tissue T_1 value, such as the myocardial muscle tissue, and only for one imaging time point. Thus, the approach has two major disadvantages. First, multiple heart phase imaging is impossible. Second, the tagging contrast becomes poor due to the longitudinal relaxation of the tissue below and above the isolated slice, which has a different T_1 to that of the myocardium. This fact is very important as the heart especially in patients suffering from cardiac disease is often surrounded by fat tissue.

A new myocardial tagging sequence for true projection myocardial tagging is proposed, which is based on the complementary spatial modulation of the magnetization technique (10), or CSPAMM, and which makes use of a slice-following procedure. The technique does not use presaturation pulses, and can be applied in combination with any multiple heart phase imaging sequence. To produce polar coordinate tags (11), it has been shown that SPAMM can be applied slice selectively perpendicular to the imaged plane. Slice-following is performed by tagging only a thin slice, parallel to the imaging plane, instead of the whole volume (12). The slice thickness for the imaging procedure is chosen sufficiently large to encompass the extent of the tagged slice's displacement. Due to the inherent properties of CSPAMM, relating to the subtraction of two different tagged measurements, an image of the thin tagged slice is automatically obtained.

In the next section the theoretical basics for the new approach are given. Some emphasis is put on the data acquisition strategy involving two one dimensionally tagged reduced k space images, an approach that may considerably shorten the examination time. Then the implementation of the technique on a 1.5 T whole body system (Philips Gyroscan ACS II), and a breathhold scheme for the elimination of respiratory artifacts are

MRM 31:401–413 (1994)

From the Institute of Biomedical Engineering and Medical Informatics, University of Zurich, the Swiss Federal Institute of Technology, Zurich, Switzerland, Department of Radiology, University Hospital, Zurich, Switzerland (G. C.M.), and Philips Medical Systems, Best, The Netherlands (W.P.).

Address correspondence to: P. Boesiger, Ph.D., Institute of Biomedical Engineering, and Medical Informatics, University and ETH Zurich, Gloriastrasse 35, 8092 Zurich, Switzerland.

Received July 13, 1993; revised December 8, 1993; accepted December 9, 1993.

This work was supported by the Swiss Commission for Promotion of Scientific Research (KWF).

0740-3194/94 $3.00

described. The improvement to be obtained with a surface coil compared with a body coil are also documented. Finally, the relevance of this work with respect to the noninvasive determination of the myocardial motion is examined.

METHODS AND MATERIALS

Slice-Following Principle

Assume a one-dimensional imaging situation, as shown in Fig. 1, for an xz plane, where z is the slice-selection direction, and x, the read-out or tagging direction. In contrast to previous tagging sequences, the spatial modulation of the magnetization is not applied to the whole volume of the myocardium but, rather, restricted to a thin slice of thickness s_t. For all heart phase images, the signal from a volume, which is delimited by a_l and a_u, is acquired. Denote the steady-state magnetization, before the application of the one-dimensional tagging function, by $M_{ss}(x,z)$. The tagging function TAG(x,z) is always between −1 and 1. Further denote the magnetization outside the tagged slice, which may also be influenced by the tagging sequence but is not tagged, by $M_{VO}(x,z)$. The z magnetization after the application of the tagging sequence is then given by

$$M_z(x, z, t = 0) = \begin{cases} M_{ss}(x, z)\mathrm{TAG}(x, z) & \text{for } -s_t/2 \le z \le s_t/2, \\ M_{V0}(x, z) & \text{otherwise.} \end{cases} \quad [1]$$

During a time interval t_k, before the k-th imaging RF excitation pulse is applied, the z magnetization experiences longitudinal relaxation, described by the relaxation time T_1, and an additional reduction due to the excitations of the previous imaging RF excitation pulses. Furthermore, the tagged slice is displaced and deformed such that the upper and lower limits $s_u(x,t_k)$ and $s_l(x,t_k)$, respectively, change their positions in the imaged volume. In the image acquisition part of the sequence, a volume of thickness large enough to encompass the extent of the displacement of the tagged slice is excited using an RF excitation pulse of flip angle α_k. Assuming that s_l and s_u lie always between a_l and a_u, and neglecting relaxation effects between the RF excitation and the signal acquisition, the measured signal $I_k(x)$ is proportional to the transverse magnetization of the entire volume

$$I_k(x) \propto \sin(\alpha_k) \int_{a_l}^{a_u} M_z(x, z, t_k)\, dz. \quad [2]$$

The magnetization of Eq. [2] can be decomposed into a "tagged" and a "nontagged" part. The tagged magnetization, Q_k, is that from the initial thin tagged, and now displaced, slice. The nontagged magnetization, consisting of two parts, m_{Rk} and m_{Vk}, comes from the entire imaged volume. Thus,

$$I_k(x) \propto \sin(\alpha_k)\left\{ m_{Rk} + m_{Vk} + \int_{s_l(x,t_k)}^{s_u(x,t_k)} Q_x(x, z)\, dz \right\}. \quad [3]$$

The nontagged magnetization components are derived from the relaxed magnetization of the tagged slice (m_{Rk}), and from the magnetization of the tissue below and above the tagged slice (m_{Vk}). For a detailed description of Q_k, m_{Rk}, and m_{Vk}, refer to the Appendix. Using the CSPAMM

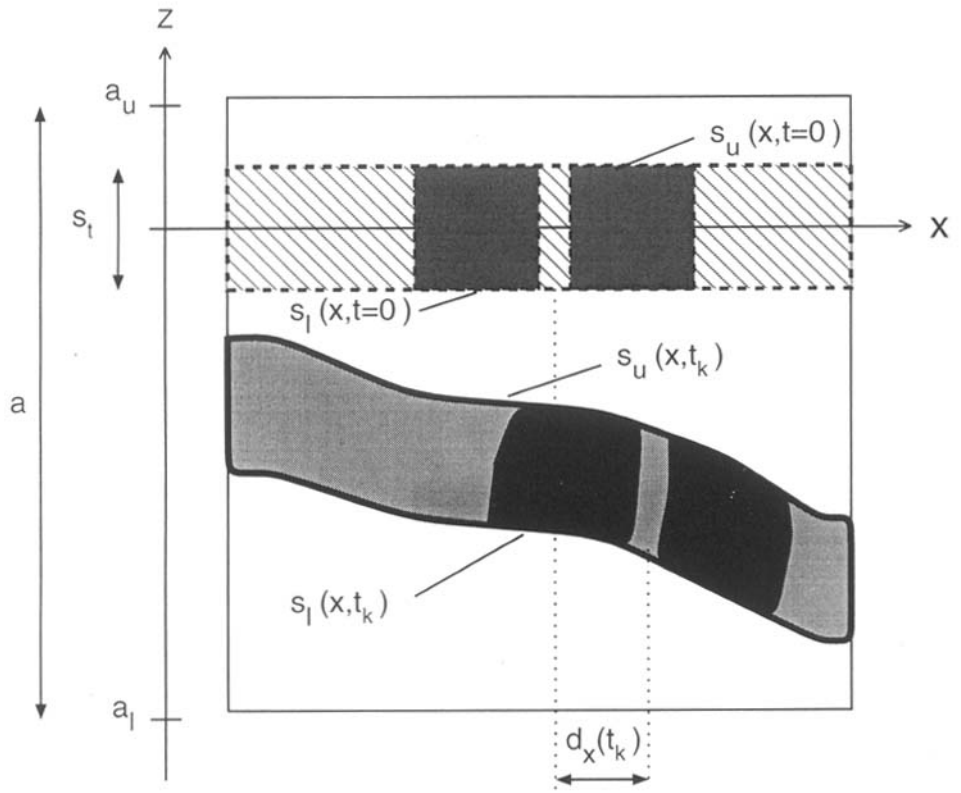

FIG. 1. Schematic view of the tagging situation immediately after the application of the tagging sequence and after a time interval t_k within a thick imaged slice. The initially tagged slice (dashed area) is translated and deformed during t_k due to in-plane motion as well as the through-plane motion.

approach (10), signal from the tagged component of the magnetization, Q_k, can be separated from the nontagged signal components. To this end, two images, I_{Ak} and I_{Bk}, have to be acquired, whereby for the second measurement the sinusoidal magnetization modulation function is negated with respect to the first. The application of a 180° phase shift to the tagging function yields minus Q_k. The subtraction of both images gives an image of only the tagged thin slice. That is

$$I_{Ak}(x) - I_{Bk}(x) \propto 2 \sin(\alpha_k) \int_{s_l(x,t_k)}^{s_u(x,t_k)} Q_k(x, z)\, dz. \quad [4]$$

As the value of an image pixel is proportional to the integral along the z axis, this image is a projection of the deformed thin tagged slice onto the xy plane. Thus, the assessed displacement of a labeled point is the projection of the three-dimensional displacement onto the xy plane (see Fig. 1, $d_x(t_k)$). The tag's displacement in Fig. 1 shows just the x component of the true three-dimensional displacement $[d_x(t_k),d_y(t_k),d_z(t_k)]$. Using two measurements of the same slice, perpendicular to the z axis and with orthogonal stripe patterns, the displacements $d_x(t_k)$ and $d_y(t_k)$ can be measured directly. The component $d_z(t_k)$ can be acquired from an orthogonal image, with the tagging direction parallel to the z direction. The three-dimensional displacement assessed by this procedure is not an approximation but a direct determination without requiring interpolation and the calculation of the labeled point's position in the reverse time direction.

The tagging pulse sequence for the assessment of the true projection of the three-dimensional motion is shown in Fig. 2. The first 90° RF pulse β_1 of the tagging sequence together with the gradient G_S selects the thin slice. The spatial modulation of the magnetization is induced by the tagging gradient G_t. The second 90° RF pulse β_2 rotates the modulated transverse magnetization back to the

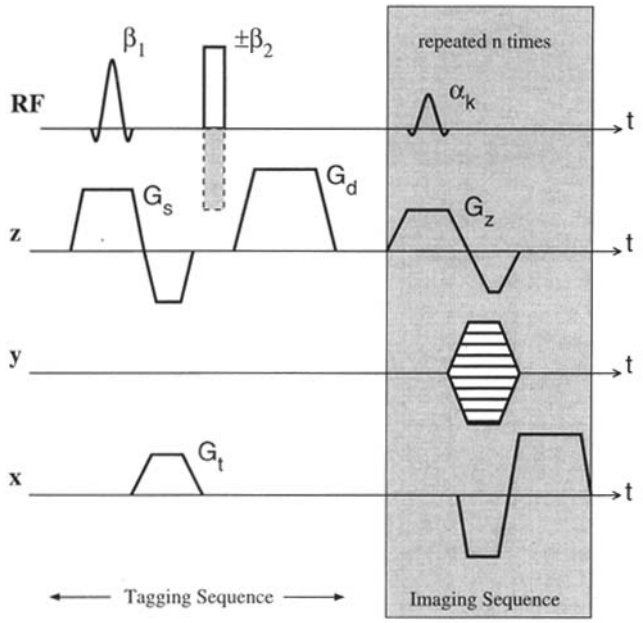

FIG. 2. slice-following CSPAMM tagging sequence.

z direction. A 180° phase shift of this pulse yields the negation of the tagging function. Before the imaging sequence is applied, the remaining transverse magnetization is spoiled by the gradient G_d. The RF pulse β_2 can also be applied selectively to the same slice as β_1, such that the tagging sequence does not influence the magnetization outside the selected tagged slice. However, the nonselective application of this pulse yields a simultaneous 90° presaturation of the nontagged tissue, thus improving the signal ratio between the desired and the acquired signal for the early heart phase images.

The volume that is selected for imaging by the excitation RF pulse α_k and the gradient G_z, is much larger than the tagged volume. However, in order to optimize the ratio of the desired to the acquired signal, the imaged volume should be made as thin as possible. Note that it is not necessary for the imaged and the tagged slice to have the same z off-center values. The imaging sequence is repeated for n heart phases. Further, note that the imaging RF excitation pulse angles do not have to be constant during the imaging sequence, a point discussed later.

K Space Reduction

The patient examination time can be reduced by acquiring two images with orthogonal one-dimensional stripe patterns, rather than the direct acquisition of an image with a two-dimensional grid pattern. The number of k space profiles per stripe image can be considerably reduced without loosing spatial precision of the tagged structure if the direction of the tagging gradient G_t and the read-out direction for the imaging procedure are identical. Figure 3 compares the k spaces of a cylindrical phantom image for a) a two-dimensional 1–4–6–4–1 SPAMM (13) and b) a one-dimensional 1–1 SPAMM image (SPAMM = SPAtial Modulation of the Magnetization). The x axis denotes the read-out and tagging direction. On the k space of the 1–1 SPAMM image two bright dots on the x axis are observed. They are the convolution products of the frequencies of the anatomical structures of the image and of the spatial modulation of the magnetization. The same convolution products can be seen on the k space image for the two-dimensional tagging sequence, but here they are spread in both the x and y directions. The additional convolution products on the axis are due to the higher harmonic frequencies in the tagging grid. A 1–4–6–4–1 SPAMM sequence produces the fundamental grid frequency and the first three harmonics (whereas a 1–1 SPAMM sequence only produces the fundamental component). As the two-dimensional tagging grid is a multiplication in the image domain of two one-dimensional striped patterns, off axis convolution products, again in the spacing of the grid fundamental frequency, are apparent. The deformation of the tagged structures causes the areas around the modulation components to become less distinct.

To obtain the full tagging information, the whole k space has to be sampled in the two-dimensional modulated case. In contrast with the one-dimensional tagging case, the acquisition of about 25%, or even less if using half k space acquisition, of the k space profiles is sufficient. Assuming a maximal rotation of the endocardium

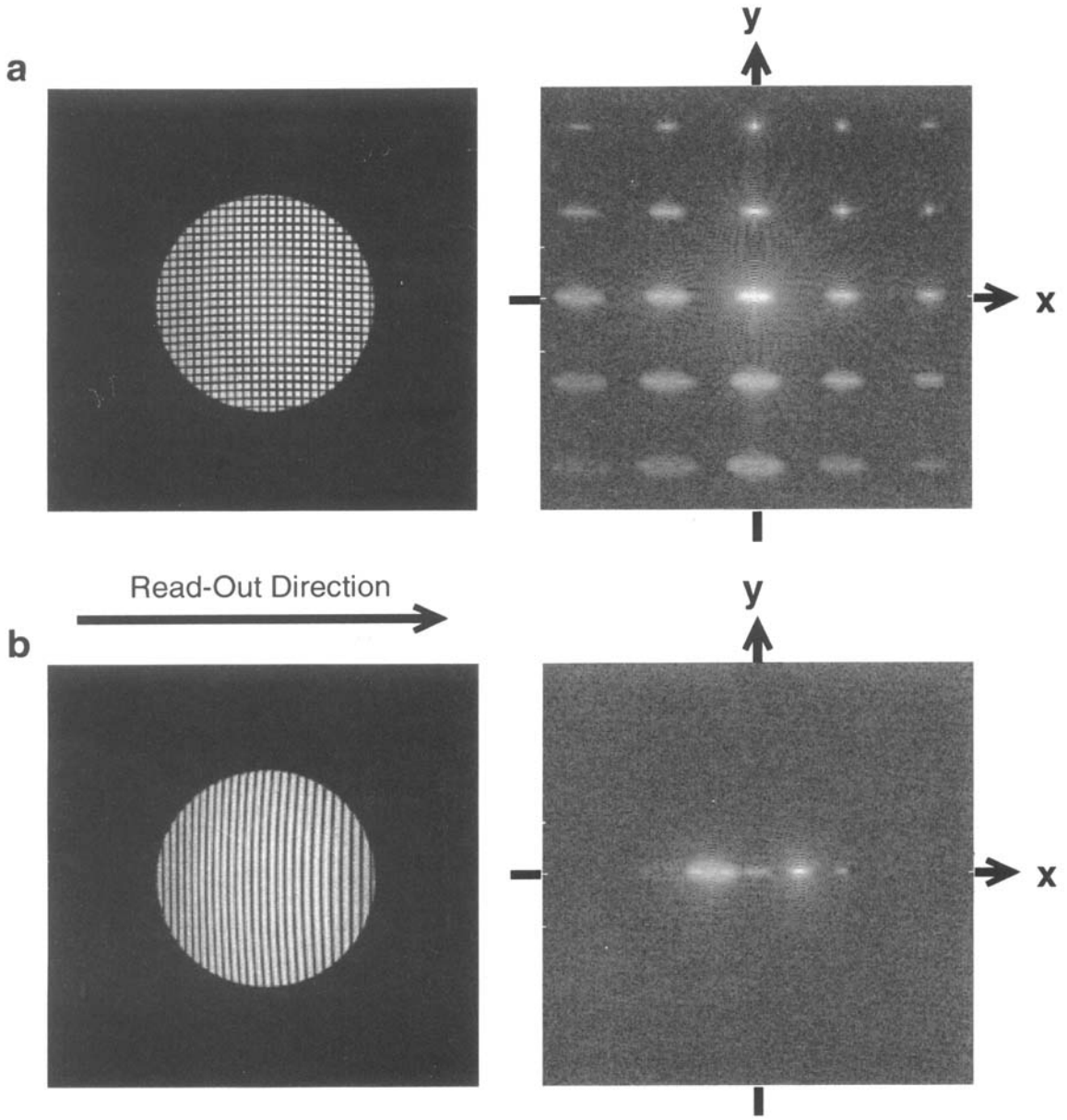

FIG. 3. Comparison of (a) a *k* space of a two-dimensional 1–4–6–4–1 SPAMM image and (b) of a one-dimensional 1–1 SPAMM image of the same cylindrical phantom.

at an apical level of 30° (5), the modulated frequency component of that part of the image also rotates 30° around the center of the *k* space. A reasonable fundamental frequency of the spatial modulation of the magnetization is 1/5 of the maximal read-out frequency (14). In this case even the frequencies up to the first harmonic of the modulation frequency of the 30° rotated image part is still within the 25% center *k* space profiles.

This *k* space reduction decreases the resolution parallel to the stripes. However, the resolution perpendicular to the stripes, which is important for a precise identification of the grid lines, is not influenced. For the acquisition of the second image, which is modulated with a perpendicular stripe pattern, the read-out and the preparation direction have to be changed. Finally, the two images with orthogonal stripe patterns are multiplied to obtain an image with a two-dimensional tagging grid.

In addition to the reduced measurement time, there are further advantages with this technique. First, the images with the one-dimensional stripe patterns can be analyzed directly with an automatic grid line detection algorithm. The identification and tracking of the grid lines are much easier than the identification and tracking of the intersection points of a two-dimensional grid. Second, even on thin tissue structures, such as the right ventricular heart wall or the left ventricle of a patient after an infarction, stripes in at least one direction can be observed. In this case the myocardium itself can give the "tagging" information in the second dimension, and allows one to assess the two-dimensional motion. Third, the one-dimensional tagging sequence is shorter compared with a two-dimensional sequence, and finally the total amount

of signal yielding the image is increased.

Implementation

The sequence was implemented on a 1.5 T whole body system, Gyroscan S15/ACS (Philips Medical Systems, Best, The Netherlands). The tagging sequence is applied immediately after the detection of the R wave of the electrocardiogram (ECG). The imaging sequence is a standard gradient echo sequence (FFE - Fast Field Echo) (15). However, the imaging RF excitation angles α_k are increased from one image to the next one during the heart period in order to obtain a constant amplitude of the tagged component of the transverse magnetization for all heart phases. A similar optimization was proposed for echo planar imaging (16) and for imaging with stimulated echoes (17). As the observation period in the tagging application is long compared with T_1, the imaging RF excitation angles are optimized additionally with respect to the T_1 relaxation time of the myocardium (10), according to

$$\alpha_{k-1} = \arctan\left(\sin(\alpha_k)e^{-\frac{t_k - t_{k-1}}{T_1}}\right), \quad [5]$$

with the condition that for the last image of the heart phase series $\alpha_n = 90°$. T_1 for myocardial muscle tissue was estimated to be 850 ms (18). The echo time was 6 ms, the tagging grid spacing was 7 to 8 mm.

By implementing the second tagging pulse β_2 as a slice-selective pulse in the phase-encoding direction (Fig. 4), fold-over artifacts are suppressed. The frequency of the RF pulse has to be chosen such that the excited volume sufficiently encompasses the heart. Thus, only the magnetization within a region of interest is spatially modulated and the magnetization outside this region is equal for both measurements, I_{Ak} and I_{Bk}, and therefore suppressed in the subtraction image. Hence, the field-of-view can be reduced, which results in a reduction in examination time.

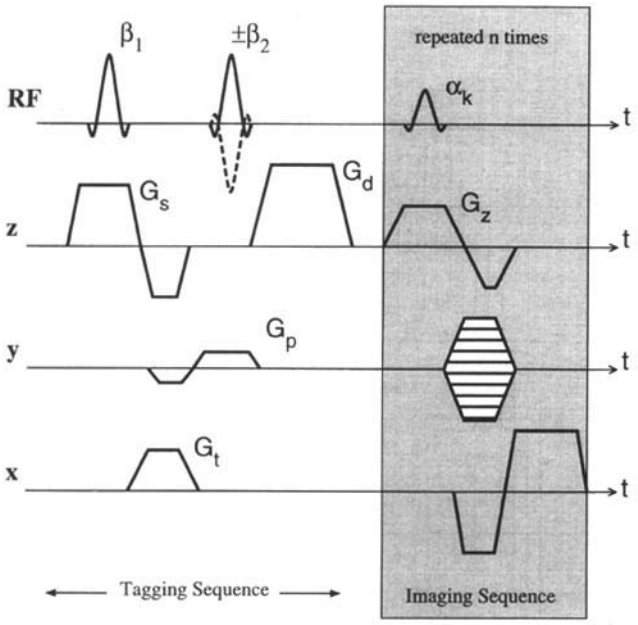

FIG. 4. slice-following/fold-over suppression CSPAMM tagging sequence.

Figure 5 shows the same two equatorial short-axis slices of a healthy volunteer at end-diastole without (Fig. 5a) and with (Fig. 5b) the extension for fold-over suppression. The nontagged components of the image are very well suppressed.

Breathhold Scheme

Subtraction techniques are more sensitive to motion artifacts when compared with normal imaging. In addition cardiac images in general suffer from the respiratory motion. Figure 6 shows a systolic short-axis image of a healthy volunteer using the slice-following sequence, incorporating fold-over suppression. Many signals due to motion artifacts in the nontagged area are visible. Here, a reduction of the field-of-view would lead to fold-over artifacts as the signal outside the region of interest is not very well suppressed. Most artifacts appear parallel to the stripes in the phase-encoding direction and do not disturb the tagging pattern on the myocardium. Swapping read-out direction and preparation direction changes the motion artifacts. Thus, the multiplication of the two images with perpendicular stripe patterns tends to suppress a large amount of motion artifact (cf. Fig. 8).

In order to suppress respiratory artifacts, a breathhold scheme, which has initially been developed for MRA of the coronary arteries (19), was applied. The breathhold recovery cycle is matched to the individual breathing rhythm. At the end of each exhalation, the tagging and imaging sequence is synchronized to the ECG's R wave. Data are acquired only during one heart beat. For each heart phase image, one phase-encoding step is performed. The patient is then given about 3 s (3 heartbeats) to inhale slightly, to exhale, and to wait for the next acquisition step. With this procedure the examination time/slice is increased by a factor of four in comparison with a acquisition without breathholding. However, no breathing recovery time for the patient is required between the scans. An advantageous characteristic of this technique is the increased magnetization recovery time between the subsequent acquisition steps. Thus, the steady-state magnetization, immediately before the application of the tagging grid, is nearly equal to the thermal equilibrium magnetization.

RESULTS

Simulations

Another problem of the subtractive slice-following technique is that the ratio between the wanted and the unwanted signal component becomes poor at later heart phases. To further elucidate this problem, a numerical solution of the signal components of Eq. [3] was performed with parameter sets of true myocardial motion tracking experiments. For compactness we define

$$m_{Qk} = \int_{s_l(x,t_k)}^{s_u(x,t_k)} Q_k(x, z)\, dz. \quad [6]$$

The simulation was performed based on a uniform phantom with a T_1 of 850 ms. Figure 7 shows the result obtained

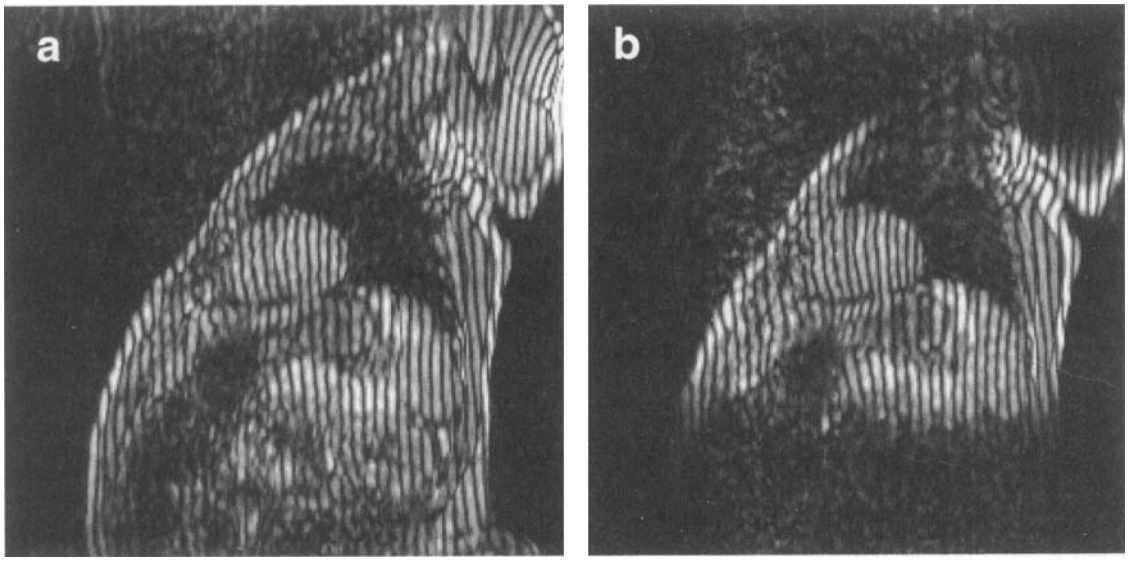

FIG. 5. End-diastolic short-axis images of the equatorial level of a healthy volunteer without (a) and with fold-over suppression (b). The tagged slice thickness is 8 mm, the thickness of the imaged volume is 30 mm.

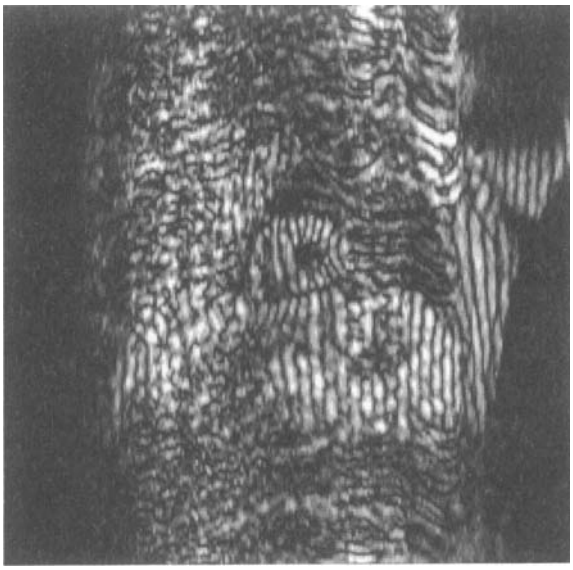

FIG. 6. Equatorial short axis of a healthy volunteer 175 ms after the R wave. The slice-following/fold-over suppression tagging technique was applied combined with an FFE imaging sequence using the system's body coil and no breathhold scheme.

with the same imaging parameters as used for the acquisition of the images in Fig. 12. The imaged slice thickness is 30 mm, the tagged slice thickness is 5 mm, 16 heart phases are measured with an interval time of 35 ms. The multiple heart phase sequence was repeated every 4 s in modeling a heart beat rate of 60 beats/min, and the previously described breathhold scheme. The relative composition of the acquired signal I_k, containing the tagged magnetization integrated over the initial selected slice m_{Qk}, the relaxed signal of the tagged slice, m_{Rk}, and the remaining signal from the imaged volume, m_{Vk}, is plotted for the 16 heart phases, $k = 1..16$. The absolute amplitude of the excited tagged transverse magnetization, $m_{Qk} \sin \alpha_k$, is constant for every heart phase, in this case 17.5% of the thermal equilibrium magnetization, as variable imaging excitation flip angles are used according to Eq. [5]. The second RF pulse β_2 of the tagging sequence is applied nonselectively yielding a suppression of the component m_{Vk} for the first images. The signal acquired for the first image is only induced by the tagged magnetization. The tagged compartment of the imaged signal then decreases dramatically for successive heart phases, resulting in a tagged signal component of less than 10% for the last image. The nontagged signal components are suppressed due to the subtraction procedure. However, the increasing unwanted signal components of the later images decrease the signal-to-noise ratio (SNR). Also, the signal from regions where the subtraction procedure fails, such as around the aorta, is increased in the same manner as the unwanted magnetization of Fig. 7. In such a case the application of spatially selective presaturation pulses before the imaging excitation helps to suppress such regions.

Body Coil Imaging

Initially the technique was applied using the system's body coil for both the transmission and the reception of the RF signals, without the application of a breathhold scheme. Figure 8 shows four out of six equatorial heart phase images of a volunteer obtained by the multiplication of two orthogonal one-dimensional sets of tagged stripe images. The thickness of the imaged volume was 30 mm, FOV 400 × 400 mm, whereby only an 8-mm thin slice was tagged. ECG-triggering, but no respiratory gating or respiratory k space profile ordering, was applied. The short-axis view is zoomed to a 100 × 100 mm region of interest. The time interval between two subsequent heart phase images was 75 ms. The first image (top left) was acquired immediately after the application of the tagging sequence, 25 ms after the detection of the R wave of the ECG. The fact that the blood within the ventricles, displaced since the application of the tagging grid, is still visible in the image acquired 100 ms after the R wave (top

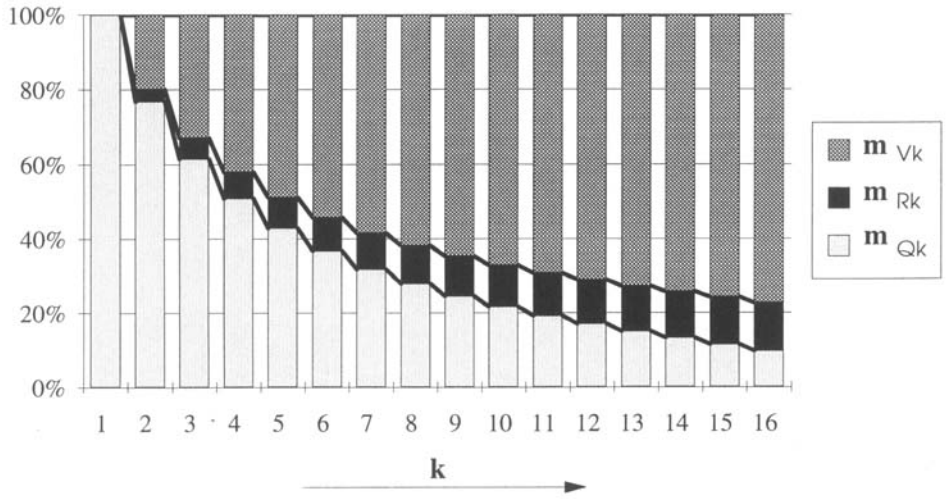

FIG. 7. Simulation of the relative distribution of wanted tagged magnetization component m_{Qk} (lowest bars), and unwanted signal. The unwanted signal is decomposed into m_{Rk} (black) from the relaxed component of the magnetization and into m_{Vk} (cross hatch) from the nontagged magnetization from imaged volume.

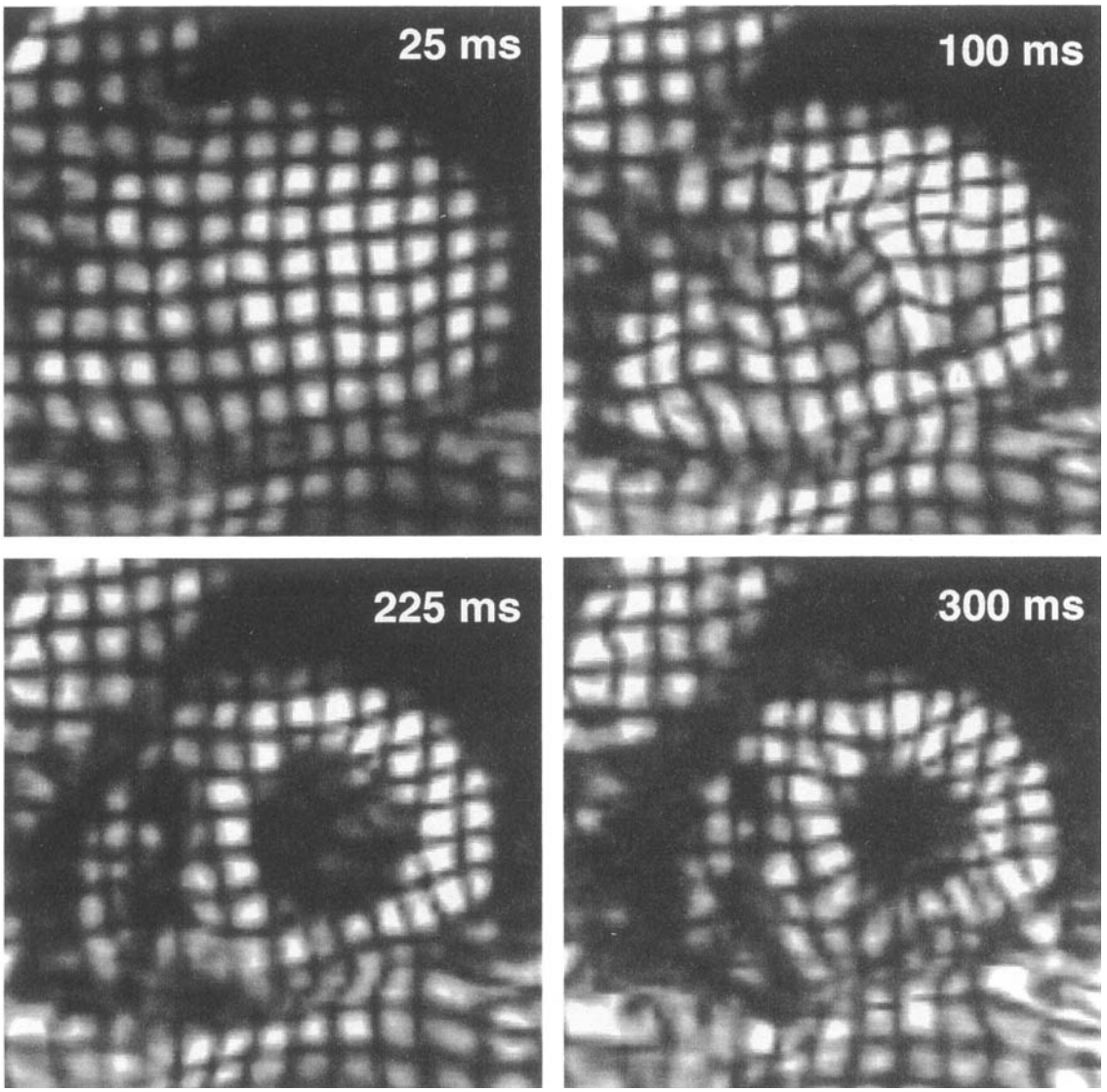

FIG. 8. Four out of six tagged heart phase images of the equatorial short-axis plane of a healthy volunteer. The shown images are acquired at 25, 100, 255, and 300 ms after the detection of the R wave of the ECG.

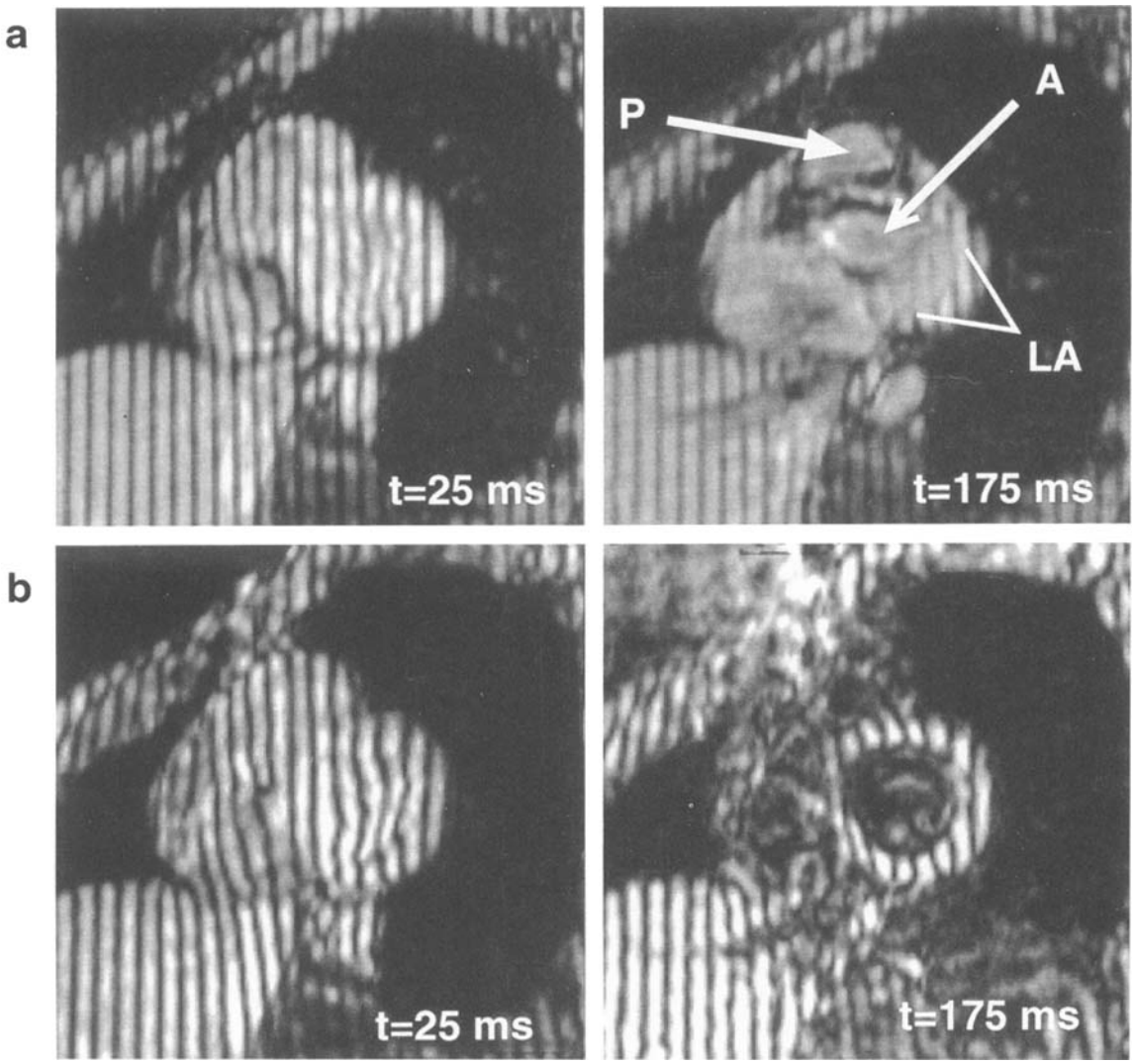

FIG. 9. Comparison of a conventional 1–3–3–1 SPAMM image obtained with the slice selective imaging sequence (a) and the slice-following tagging technique (b). The left column shows the same basal short-axis slice of a healthy volunteer at end-diastole. The right column shows images of the same time series 175 ms after the R wave.

right), indicates that the slice-following procedures works successfully. A further indication that an initially tagged slice is being followed is that even the right ventricle is clearly visible on the image at $t = 225$ ms (bottom left), and on the end-systolic image ($t = 300$ ms, bottom right). The tagging contrast is sufficient for an automatic detection of the intersection points of the grid, and stable from end-diastole to end-systole.

The effect of slice-following is also clearly demonstrated on the images of a top basal short-axis slice. Figure 9 shows the difference between a conventional a) 1–3–3–1 SPAMM sequence (upper row) and b) the slice-following CSPAMM tagging technique (lower row). The first column shows the same basal short-axis slice of a healthy volunteer. At the top, the slice is selected with an imaging slice thickness of 8 mm. Exactly the same slice position is selected for the selective tagging procedure with identical tagging slice thickness of 8 mm but an imaging slice thickness of 30 mm. The second column shows the images acquired 175 ms after the R wave. The myocardium of the left ventricle in the upper row has already disappeared from the static imaged slice modulated with a conventional SPAMM sequence. Tagged tissue of the left atrium (marked with LA), the pulmonary artery (P) and the aorta (A) have been moved into the imaged slice. In the case of the followed slice, the whole left ventricle remains visible. However, some tagged tissue, such as the right ventricle, and blood within the ventricles are no longer visible. These components have moved completely out of the imaged volume.

Body Coil and Breathhold Imaging

Figure 10 shows three heart phase images of a top basal short-axis slice of a volunteer obtained with the system's body coil in conjunction with the application of the breathhold scheme described previously. Using an end-diastolic long-axis image, the slice for the tagging procedure was selected just below the valves between left atrium and left ventricle, with a slice thickness of 8 mm.

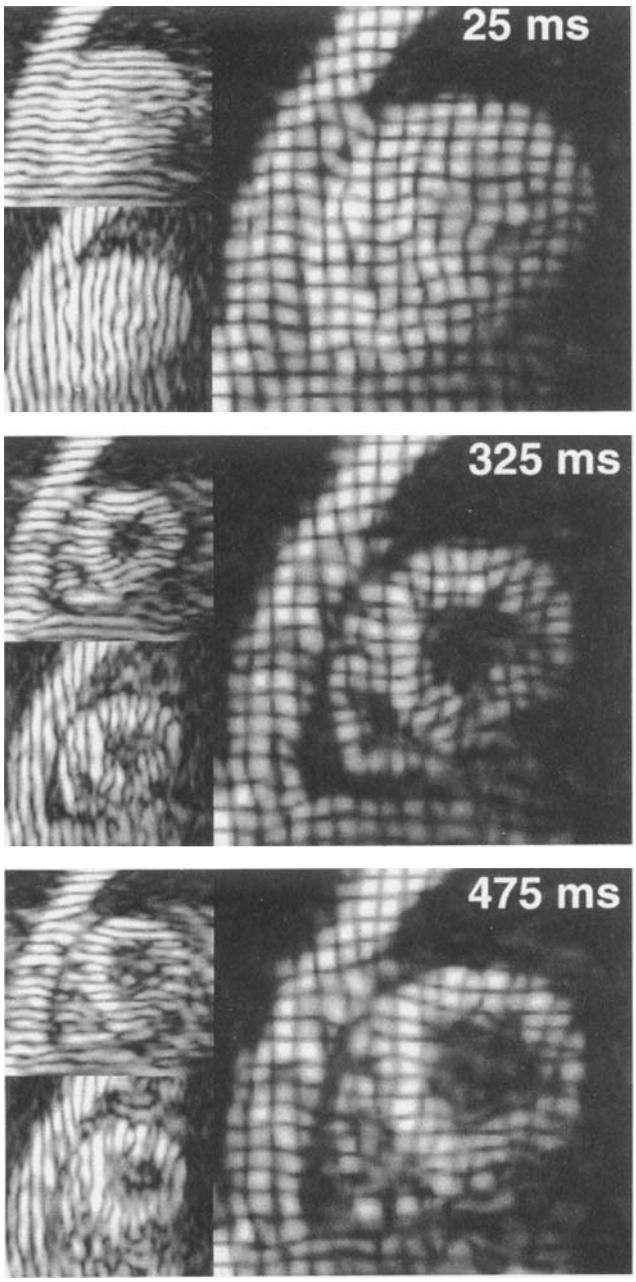

FIG. 10. Three out of 10 short-axis images of a voluntéer of a top basal slice. The images are acquired at end-diastole (left), at end-systole (middle), and at 475 ms after the R wave of the ECG.

The 40-mm thick volume selected for imaging was positioned such that the upper boundary (nearest to the atria) is at the same level as the upper boundary of the tagged slice. Ten images were obtained with an interval time of 50 ms. Figure 10 shows the end-diastolic, the end-systolic, and the very last image, at t = 475 ms after the R wave, of this series. Even the tagged right ventricle is clearly visible on the end-systolic image. The image improvement due to the application of the breathhold scheme can be seen with respect to Fig. 9. The major disadvantage of this measurement protocol is the long scan time. About 10 min, or 640 heart beats, are needed for the acquisition of the full tagging information/slice ($2 \times 2 \times 40 \times 4 = 640$; 2 spatial directions, positive and negative grid, 40 k space profiles, four heart beats).

Surface Coil and Breathhold Imaging

Using a commercially available surface coil (ϕ = 20 cm, C1, Philips Medical Systems Best, The Netherlands) and the previously described breathhold scheme, not only the motion artifacts are reduced but also the SNR is significantly increased. Figure 11 shows three out of 10 image sets, each consisting of the two acquired images with the one-dimensional tagging patterns, and the multiplication image. The time interval between the 10 images was held constant at 50 ms. The first image set was acquired at end-diastole 25 ms after the R wave of the ECG, the second at end-systole, and the third 475 ms after the R wave at early mid-diastole. The tagging contrast and the SNR is stable during the entire cardiac cycle. The suppression of motion artifacts is mainly due to the application of the breathhold scheme but also due to the multiplication of the two one-dimensional tagged images. The excellent SNR over the whole sequence is due primarily to the variable imaging excitation pulse angle in conjunction with the application of a surface coil. A problem with surface coils for cardiac applications is the reduced sensitivity in the lateral segment of the left ventricle. However, as demonstrated in Figs. 11 and 12, the SNR generally is sufficient at an apical and an equatorial level of the heart, which makes an accurate grid intersection point identification possible.

Figure 12 shows a series (Figs. 12a–12p) of 16 apical short-axis slices of a volunteer acquired with an interval time of 35 ms. The mean RR interval of this subject was 750 ms. The last image (Fig. 12p) was obtained at 550 ms after the R wave. Assuming that the contraction of the atria starts about 200 ms before the R wave, the entire cardiac cycle from end-diastole to the very late diastole is assessed. This is supported by the fact that the left ventricular myocardium in the last three images (Figs. 12m–12o) makes no dilatory motion. In this case the last image (Fig. 12p) is acquired after the P wave of the subsequent heart beat. A slight dilatation in the posterior segment can be observed. However, as this motion, which is due to the contraction of the atria, is not synchronous to the former heart beat, the image quality is degraded. A sufficient image quality during this period of the cardiac cycle is only achieved if the heart beat variability of the subject is small.

Tag Persistence

The tag persistence is strongly dependent on the number of excitations, on the longitudinal relaxation of the myocardial tissue, and on the signal-to-noise ratio of the images.

So far, 20 healthy volunteers and patients, aged 25 to 85, were examined with the described technique using either the body coil (n = 9) or the surface coil (n = 11). When the body coil was used, the tags could be tracked up to 750 ms after the application of the tagging grid. However, in this case the number of heart phases was always set to be seven and the interval time between the heart phase images was chosen such that the forth image

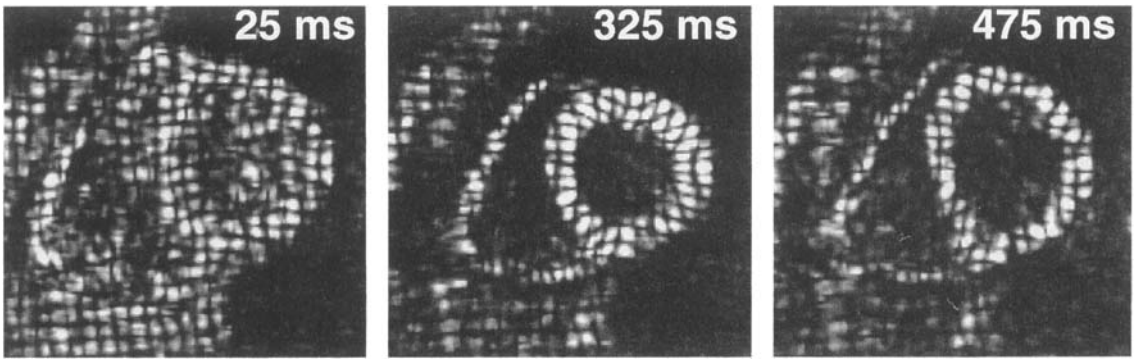

FIG. 11. Three out of ten equatorial short-axis images of a healthy volunteer. For end-diastole (first image set of the series), end-systole, and mid-diastole (last image set of the series) the measured one-dimensional tagged images and the multiplication image is shown. The heart phase interval time was 50 ms and a standard surface coil (ϕ = 20 cm) was applied for the reception of the RF signals. The tagged slice thickness was 5 mm, whereby the imaged volume had a thickness of 30 mm.

was acquired at end-systole. In all the cases the stripe patterns could be tracked up to the last image. Usually the stripe images in one direction showed less motion artifacts than the images in the other in-plane direction of the same slice.

Using the surface coil the heart phase image interval was always set at 35 ms. Dependening on the heart beat rate, 16 to 18 images were acquired. In all cases the heart motion could be assessed during the entire time series at least at apical and equatorial level. In seven cases the sensitivity of the surface coil was sufficient even for the basal level of the heart.

Furthermore, the examinations demonstrate that the limitation of the observation period and of the temporal resolution of the described method is mainly due to motion artifacts and not due to the fading of the tags. Motion artifacts were observed if the breathhold scheme was not properly performed or if the heart beat rate was strongly irregular.

DISCUSSION AND CONCLUSIONS

The use of modulus images makes myocardial tagging insensitive to phase artifacts, and the displacement of tagged points can be assessed directly in comparison with phase contrast methods (20), whereby the velocity has to be integrated over time to obtain the displacement map of the myocardium. However, the major criticisms of the myocardial tagging technique are that the entire cardiac cycle is not accessible in one imaging cycle, and that the through-plane motion makes the tagged images difficult for a direct interpretation. We have demonstrated that with the slice-following CSPAMM technique both of these limitations are no longer true.

"Tagging" implies the marking of certain areas of tissue and the following of the tissue markers through space and time. Our approach to tissue tagging comes very close to this pedantic interpretation. Here, we have only explicitly demonstrated the measurement of projected three-dimensional displacement into a plane. However, the possibility to obtain true projection motion data has important consequences for the acquisition of the three-dimensional myocardial motion data. Each of the striped images gives one dimension of the displacement. Thus, three-dimensional displacement information can be derived from three orthogonal sets of multiple slice images, with each set tagging an orthogonal one-dimensional stripe pattern. Projections of the three-dimensional motion can then be combined to achieve the true three-dimensional displacement of the selected point, without interpolation and without the need to perform a tag identification procedure in the reverse time direction.

Excluding fully three-dimensional imaging strategies, slice-following is the only way to acquire accurate short-axis images of the top basal plane during the cardiac cycle. Compared with the slice isolation technique (6), the subtraction method does not require any presaturation. Thus, the method can be applied in combination with any multiple heart phase imaging sequence. Furthermore, no tissue-dependent optimization is necessary.

The acquisition procedure for the tagged images has been carefully optimized. First, one has the application of the slice-following technique. This is especially apparent in the sharpness of the tagging pattern on the images of the right ventricle. This allows also the quantification of the right ventricular motion. Even if the wall thickness of the myocardium is much smaller than the tagging grid spacing, the same visible part of the stripe pattern is always imaged and can accurately be tracked. Second, because not only the nontagged tissue of the imaged volume, but also the signal induced by the relaxed component of the magnetization within the thin tagged sliced is suppressed, the tagging contrast is excellent throughout the entire cardiac cycle. Third, due to the optimization of the imaging excitation pulse angles, the SNR of the tagged images is constant from end-diastole over end-systole until late diastole.

One problem of the subtraction technique is that the ratio between wanted and unwanted signal is poor, and becomes very low at later heart phases. This also increases the influence of motion artifacts due to which a proper subtraction of the unwanted signal fails. However, the use of a surface coil and a breathhold scheme ameliorates these problems. An additional suppression of noise and motion artifacts is achieved by the multiplication of two

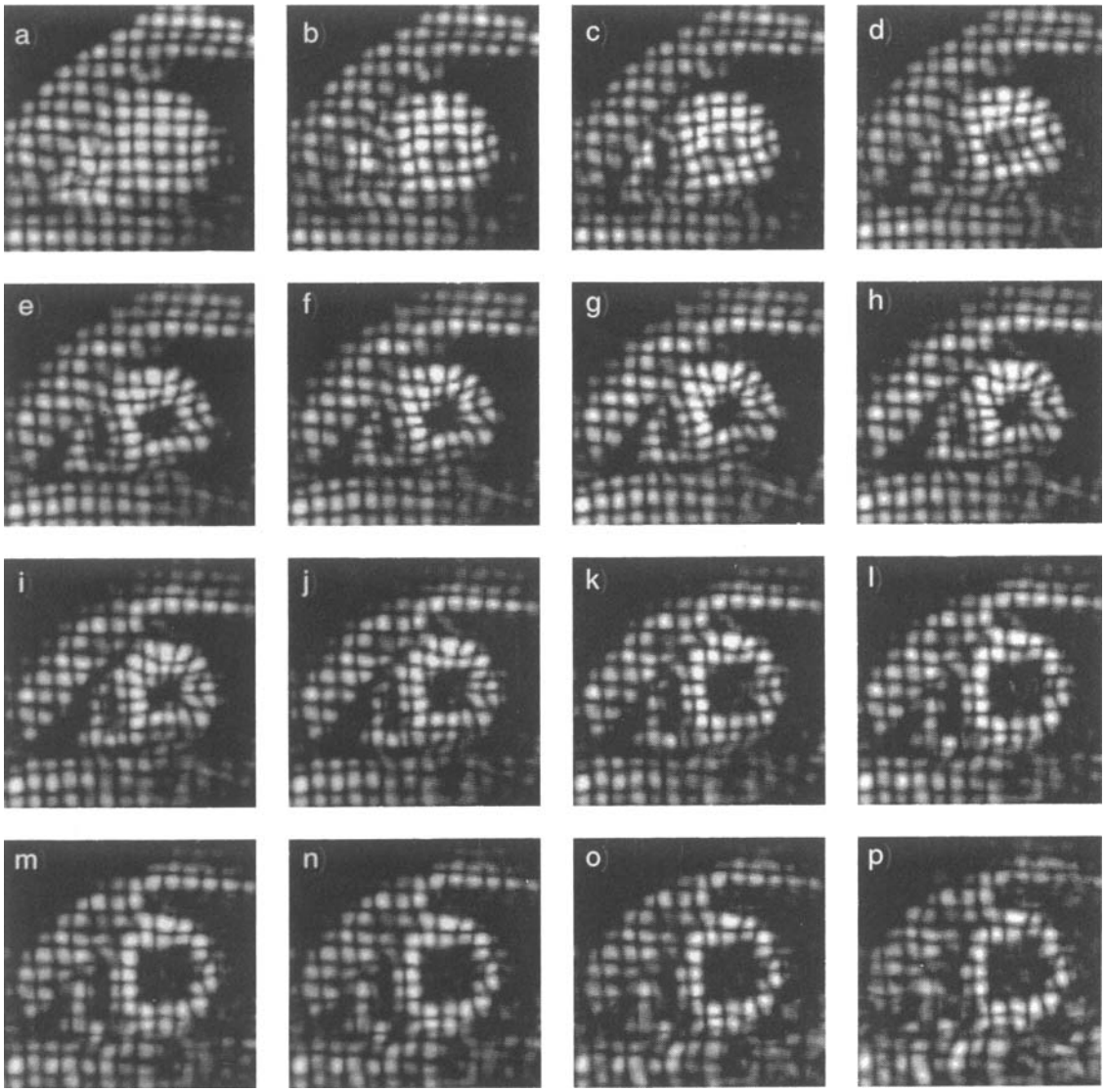

FIG. 12. Sixteen heart phase images of an apical short-axis slice of a volunteer. The heart beat rate was 75 to 80 beats/min during the examination. The time interval between the heart phase images was 35 ms.

one-dimensionally modulated images. The fact, that the read-out direction and the direction of the tagging gradient are always the same, allows one to identify the tagged structures accurately even if the number of k space profiles is extremely reduced. Thus, an important by-product of this measurement procedure is the reduction of examination time without loosing motion information.

This technique requires a long examination time if a multiple slice acquisition with orthogonal stacks of tagged images is performed. In addition to the reduced k space sampling a further reduction in the scan time can be achieved (21) by increasing the number of profiles acquired for one heart phase image within one cardiac cycle.

APPENDIX

In this appendix a detailed description of the one-dimensional imaging situation, as it is shown in Fig. 1, is given. z is the slice selection direction and x is the read-out direction, as well as the direction of the tagging gradient G_t. The acquisition part of the sequence images a volume delimited by a_l and a_u. Denote the thermal equilibrium magnetization by $M_0(x,z)$ (for simplification M_0) and the steady-state magnetization, before the application of the one-dimensional tagging function by $M_{ss}(x,z)$, or M_{ss}. The tagging function TAG(x,z) is always between -1 and 1 and normally independent on z. Further, denote the magnetization outside the tagged slice, which may be influenced by the tagging sequence but is not tagged by $M_{VO}(x,z)$. The z magnetization after the application of the tagging sequence is shown in Eq. [1].

During a time interval t_1, before the first imaging RF excitation pulse is applied, the z magnetization experiences longitudinal relaxation described by the relaxation time $T_1(x,z)$, or T_1. Furthermore, the tagged slice is displaced and deformed such that the upper and lower limits, $s_u(x,t_1)$ and $s_l(x,t_1)$, respectively, change their positions in the imaged volume. For each infinitesimally

small volume dV_i, a trajectory $r_i(t) = [x_i(t),z_i(t)]$ is assigned, starting at $r_i(t = 0) = (x_i(0),z_i(0))$. The function $\zeta_k(x,z)$ returns the starting point of the trajectory of the volume, which is located at (x,z) during the acquisition at t_k, e.g., $\zeta_k(r_i(t_k)) = [x_i(0),y_i(0)]$ and for the inverse function $\zeta_k^{-1}([x_i(0),y_i(0)]) = [x_i(t_k),y_i(t_k)]$. Thus, the longitudinal magnetization of the tagged slice is

$$M_z(x, z, t_1) = \{M_{ss}(\zeta_1(x, z))\mathrm{TAG}(\zeta_1(x, z))\, e^{-t_1/T_1} + M_0[1 - e^{-t_1/T_1}] \quad \text{for } s_l(x, t_1) \le z \le s_u(x, t_1), \quad [7a]$$

and otherwise for the nontagged volume,

$$M_z(x,z,t_1) = [M_{VO}(\zeta_1(x,z),)) - M_O]e^{-t_1/T_1} + M_O. \quad [7b]$$

In the image acquisition part of the sequence, a volume of thickness large enough to encompass the extent of the tagged slice's motion is excited using an RF excitation pulse of flip angle α_1. Neglecting relaxation effects between the RF excitation and the signal acquisition, the measured signal $I_1(x)$ is proportional to the transverse magnetization integrated over z,

$$I_1(x) \propto \sin(\alpha_1) \int_{a_l}^{a_u} M_z(x, z, t_1)\, dz. \quad [8]$$

The magnetization of Eq. [2] can be decomposed into integrals over z from the magnetization components Q_1, R_1, and M_{V1}, leading to

$$I_1(x) \propto \sin(\alpha_1)\left\{ \int_{s_l(x,t_1)}^{s_u(x,t_1)} [Q_1(x, z) + R_1(x, z)]\, dz + \int_{a_l}^{s_l(x,t_1)} M_{V1}(x, z)\, dz + \int_{s_u(x,t_1)}^{a_u} M_{V1}(x, z)\, dz, \right. \quad [9]$$

and for the k-th image acquired at t_k,

$$I_k(x) \propto \sin(\alpha_k)\left\{ \int_{s_l(x,t_k)}^{s_u(x,t_k)} [Q_k(x, z) + R_k(x, z)]\, dz + \int_{a_l}^{s_l(x,t_k)} M_{Vk}(x, z)\, dz + \int_{s_u(x,t_k)}^{a_u} M_{Vk}(x, z)\, dz. \right. \quad [10]$$

This equation is the same as Eq. [3] where the nontagged magnetization is substituted by

$$m_{Rk} = \int_{s_l(x,t_k)}^{s_u(x,t_k)} R_k(x, z)\, dz, \quad [11]$$

and by

$$m_{Vk} = \int_{a_l}^{s_l(x,t_k)} M_{Vk}(x, z)\, dz + \int_{s_u(x,t_k)}^{a_u} M_{Vk}(x, z)\, dz. \quad [12]$$

Q_k is the component of the magnetization of the tagged tissue. R_k denotes the component of the magnetization of the tagged slice, which has relaxed since the application of the tagging grid. Thus, assuming that s_l and s_u lie always between a_l and a_u, and $\alpha_0 = 0$ then

$$Q_k(x, z) = \mathrm{TAG}(\zeta_k(x, z))M_{ss}(\zeta_k(x, z))e^{-t_k/T_1} \left(\prod_{j=0}^{k-1} \cos \alpha_i\right), \quad [13]$$

and recursively, with $R_0\,(x,z) = 0$ and $t_0 = 0$,

$$R_k(x, z) = [\cos \alpha_{k-1}R_{k-1}(\zeta_{k-1}^{-1}(\zeta_k(x, z))) - M_0]e^{-(t_k - t_{k-1})/T_1} + M_0. \quad [14]$$

The z magnetization component M_{Vk} originates from the nontagged tissue below and above the tagged slice. Thus, also recursively

$$M_{Vk}(x, z) = [\cos (\alpha_{k-1})M_{Vk-1}(\zeta_{k-1}^{-1}(\zeta(x, z))) - M_0]e^{-(t_k - t_{k-1})/T_1} + M_0 \quad \text{for } a_l \le \zeta_{k-1}^{-1}(\zeta_k(x, z)) \le a_u, \quad [15a]$$

and otherwise

$$[M_{Vk}(x, z) = [M_{Vk-1}(\zeta_{k-1}^{-1}(\zeta(x, z))) - M_0]e^{-(t_k - t_{k-1})/T_1} + M_0 \quad [15b]$$

The acquired signals of both images A and B are proportional to the integral of the magnetization over z, this is for image A

$$I_{Ak} \propto \sin (\alpha_k)\left\{ \int_{s_l(x,t_k)}^{s_u(x,t_k)} Q_k(x,z)\, dz + \int_{s_l(x,t_k)}^{s_u(x,t_k)} R_k(x,z)\, dz + \int_{a_l}^{s_l(x,t_k)} M_{Vk}(x,z)\, dz + \int_{s_u(x,t_k)}^{a_u} M_{Vk}(x,z)\, dz, \right. \quad [16]$$

and for B

$$I_{Bk} \propto \sin(\alpha_k)\left\{ - \int_{s_l(x,t_k)}^{s_u(x,t_k)} Q_k(x, z)\, dz + \int_{s_l(x,t_k)}^{s_u(x,t_k)} R_k(x, z)\, dz + \int_{a_l}^{s_l(x,t_k)} M_{Vk}(x, z)\, dz + \int_{s_u(x,t_k)}^{a_u} M_{Vk}(x, z)\, dz, \right. \quad [17]$$

The subtraction I_{Ak} minus I_{Bk} finally gives an image induced only by the tissue, which was spatially modulated, as it is shown in Eq. [4],

$$I_{Ak}(x) - I_{Bk}(x) \propto \sin (\alpha_k)\left(\prod_{i=0}^{k-1} \cos \alpha_i\right) 2 \int_{s_l(x,t_k)}^{s_u(x,t_k)} \mathrm{TAG}(\zeta_k(x, z))M_{ss}(\zeta_k(x, z))e^{-t_k/T_1}\, dz. \quad [18]$$

ACKNOWLEDGMENTS

The authors thank Professors H.P. Krayenbuehl and O.M. Hess of the Cardiology Department of the University Hospital Zurich, and Dr. Stephan Maier, Brigham & Women's Hospital, Boston, for helpful discussions.

REFERENCES

1. E. A. Zerhouni, D. M. Parish, W. J. Rogers, A. Yang, E. P. Sharpio, Human heart: tagging with MR imaging—a method for noninvasive assessment of myocardial motion. *Radiology* **169,** 59 (1988).
2. L. Axel, L. Dougherty, MR imaging of motion with spatial modulation of magnetization. *Radiology* **171,** 841 (1989).
3. S. E. Maier, S. E. Fischer, G. C. McKinnon, O. M. Hess, HP. Krayenbuehl, P. Boesiger, Acquisition and evaluation of tagged magnetic resonance images of the human left ventricle. *Comput. Med. Imaging Graphics* **16,** 73 (1992).
4. N. Reicheck, Magnetic resonance imaging for assessment of myocardial function. *Magn. Reson. Q.* **7(4),** 255 (1992).
5. S. E. Maier, S. E. Fischer, G. C. McKinnon, O. M. Hess, H. P. Krayenbuehl, P. Boesiger, Evaluation of left ventricular segmental wall motion in hypertophic cardiomyopathy with myocardial tagging. *Circulation* **86,** 1919 (1992).
6. W. J. Rogers, E. P. Shapiro, J. L. Weiss, M. B. Buchhalter, F. E. Rademakers, M. L. Weisfeldt, E. A. Zerhouni, Quantification of correction for left ventricular systolic long-axis shortening by magnetic resonance tissue tagging and slice isolation. *Circulation* **84,** 721 (1991).
7. R. Unterberg, L. Plesak, W. Voelker, K. R. Karsch, Quantitative local wall motion analysis of normal right ventricle. *Z. Kardiol.* **77,** 120 (1988).
8. C. Moore, W. O'Dell, E. McVeigh, E. Zerhouni, Three dimensional myocardial strains in human using bi-planar tagged MRI, *in* "Proc., SMRM, 10th Annual Meeting, 1991, San Francisco," p. 14.
9. C. C. Moore, W. G. O'Dell, E. R. McVeigh, E. A. Zerhouni, Calculation of three-dimensional left ventricular strains from biplanar tagged MR images. *J. Magn. Reson. Imaging* **2,** 165 (1992).
10. S. E. Fischer, G. C. McKinnon, S. E. Maier, P. Boesiger, Improved myocardial tagging contrast. *Magn. Reson. Med.* **30,** 191 (1993).
11. B. D. Bolster, E. R. McVeigh, E. A. Zerhouni, Myocardial tagging in polar coordinates with use of striped tags. *Radiology* **177,** 769 (1990).
12. S. E. Fischer, G. C. McKinnon, W. Prins, P. Boesiger, True projection Tagging of the myocardium, *in* "Proc., SMRM, 11th Annual Meeting, 1992, Berlin," p. 890.
13. L. Axel, L. Dougherty, Heart wall motion: improved method of spatial modulation of magnetization for MR imaging. *Radiology* **172,** 349 (1989).
14. E. R. McVeigh, L. Gao, Precision of tag position estimation in breathhold CINE MRI: the effect of tag spacing. *in* "Proc., SMRM, 12th Annual Meeting, 1993, New York," p. 199.
15. P. van der Meulen, J. P. Groen, A. M. C. Tinus, G. Bruntink, Fast field echo imaging: An overview and contrast calculations. *Magn. Reson. Imaging* **6,** 335 (1992).
16. P. Mansfield, Spatial mapping of chemical shift in NMR. *Magn. Reson. Med.* **1,** 370 (1984).
17. J. Frahm, W. Hänicke, H. Bruhn, M. L. Gyngell, K. D. Merboldt, High-speed STEAM MRI of the human heart. *Magn. Reson. Med.* **22,** 133 (1991).
18. P. A. Bottomley, T. H. Forster, R. E. Argersinger, L. M. Pfeifer, A review of normal tissue hydrogen NMR relaxation times and relaxation mechanisms from 1–100 MHz: dependence on tissue type, NMR frequency, temperature, species, excision, and age. *Med. Phys.* **11,** 425 (1984).
19. M. B. Scheidegger, R. G. de Graaf, M. Doyle, J. Vermeulen, P. van Dijk, G. M. Pohost, Coronary artery MR imaging during multiple brief (1 sec) expiration breathholds, *in* "Proc., SMRM, 11th Annual Meeting, 1992, Berlin," p. 602.
20. N. J. Pelc, R. J. Herfkens, L. R. Pelc, 3D analysis of myocardial motion and deformation with phase contrast cine MRI, *in* "Proc., SMRM, 11th Annual Meeting, 1992, Berlin," p. 18.
21. E. R. McVeigh, E. Atalar, Cardiac tagging with breath-hold cine MRI, *Magn. Reson. Med.* **28,** 318 (1993).